In Situ Gas-Phase Hydrosilylation of Plasma-Synthesized Silicon Nanocrystals

Bhavin N. Jariwala,[†] Oliver S. Dewey,[†] Paul Stradins,[‡] Cristian V. Ciobanu,*,[§] and Sumit Agarwal*,[†]

[†]Department of Chemical Engineering and [§]Division of Engineering, Colorado School of Mines, Golden, Colorado 80401, United States
[‡]National Center for Photovoltaics, National Renewable Energy Laboratory, Golden, Colorado 80401, United States

S *Supporting Information*

ABSTRACT: Surface passivation of semiconductor nanocrystals (NCs) is critical in enabling their utilization in novel optoelectronic devices, solar cells, and biological and chemical sensors. Compared to the extensively used liquid-phase NC synthesis and passivation techniques, gas-phase routes provide the unique opportunity for in situ passivation of semiconductor NCs. Herein, we present a method for in situ gas-phase organic functionalization of plasma-synthesized, H-terminated silicon (Si) NCs. Using real-time in situ attenuated total reflection Fourier transform IR spectroscopy, we have studied the surface reactions during hydrosilylation of Si NCs at 160 °C. First, we show that, during gas-phase hydrosilylation of Si NCs using styrene (1-alkene) and acetylene (alkyne), the reaction pathways of the alkenes and alkynes chemisorbing onto surface SiH$_x$ ($x = 1-3$) species are different. Second, utilizing this difference in reactivity, we demonstrate a novel pathway to enhance the surface ligand passivation of Si NCs via in situ gas-phase hydrosilylation using the combination of a short-chain alkyne (acetylene) and a long-chain 1-alkene (styrene). The quality of surface passivation is further validated through IR and photoluminescence measurements of Si NCs exposed to air.

KEYWORDS: silicon nanocrystals, hydrosilylation, surface functionalization
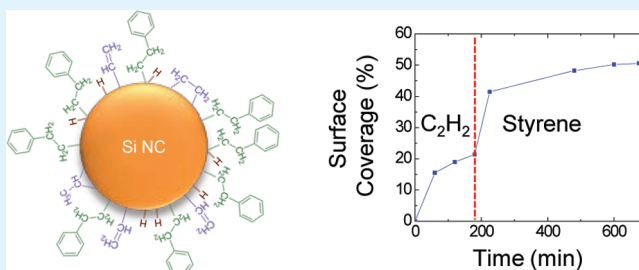
1. INTRODUCTION

Crystalline silicon (c-Si) in its bulk form is known to have relatively weak optical absorption owing to its indirect band gap. Because of quantum confinement effects, striking changes in the optical and electronic properties arise when the size of c-Si is reduced to a few nanometers.[1-5] It has been demonstrated that quantum-confined Si nanocrystals (NCs) (<5 nm) show a size-dependent band gap, which is significantly greater than that of bulk Si (~1.1 eV).[1] Moreover, unlike the bulk material, Si NCs exhibit strong visible photoluminescence (PL) at room temperature.[2,3] More recently, it was demonstrated that direct no-phonon optical transitions in Si NCs are size-dependent, and the efficiency of such transitions is ~1000 times higher than that in bulk Si.[4] Efficient multiple-exciton generation (MEG), that is, single-photon absorption resulting in two or more electron—hole pairs, has also been reported in colloidal Si NCs using ultrafast transient absorption spectroscopy.[5] These unique properties have led to major advances in demonstrating the potential use of quantum-confined Si NCs in novel optoelectronic devices such as Si NC-based lasers and light-emitting diodes.[6-8] Luminescent Si NCs have been proposed for fluorescent biological labels[9] and chemical sensors.[10,11] Properties such as MEG,[5] quantum cutting,[12] and down conversion[13] have generated interest in Si NCs as candidates for third-generation photovoltaic (PV) devices.[13,14] However, to realize the full potential of Si NCs in the above-mentioned applications, control over the NC size as well as their surface functionalization is critical.

Because quantum-confined Si NCs have a high surface-to-volume ratio, changes in both the size and surface play an important role in modifying their optical properties.[3,15] Surface oxidation of unfunctionalized Si NCs in air results in a change in their size as the oxide shell consumes the Si core. This, in turn, increases their band gap because of the reduced size and also affects the PL quantum yield and exciton lifetimes due to a modification in the surface states.[5,16] Therefore, to synthesize stable Si NCs with a low density of surface defects, various chemical passivation and functionalization techniques have been developed.[10,17,18] A key issue while performing surface chemistry on Si NCs is starting with a chemically active surface that assists in subsequent functionalization. Depending on the Si NC synthesis technique, the as-grown surface can be terminated by Si—H, Si—Cl, and Si—OH.[2,17,19] Gas-phase synthesis of Si NCs has the advantage of obtaining free-standing Si NCs with a relatively high throughput.[2,19] In particular, a continuous-flow, nonthermal, radio-frequency (rf) SiH$_4$/Ar plasma provides free-standing nanoparticles over a size range of 3—10 nm with a narrow size distribution ($\pm$10%).[2] An additional benefit derived from using a plasma-assisted technique is that the NCs are inherently H-terminated because of the abundance of atomic

Scheme 1. Two-Step Mechanism for Hydrosilylation of Si Surfaces Using 1-Alkene and 1-Alkyne
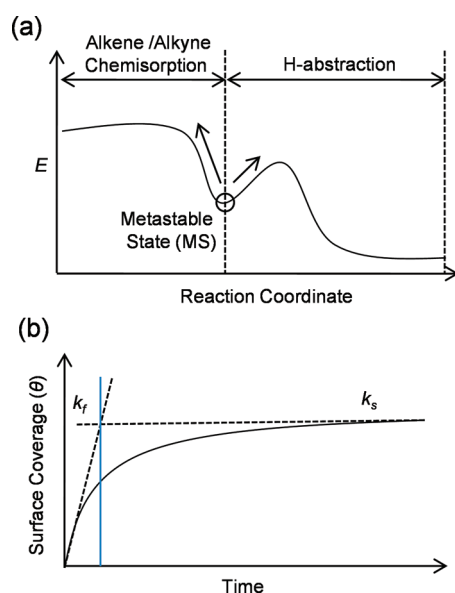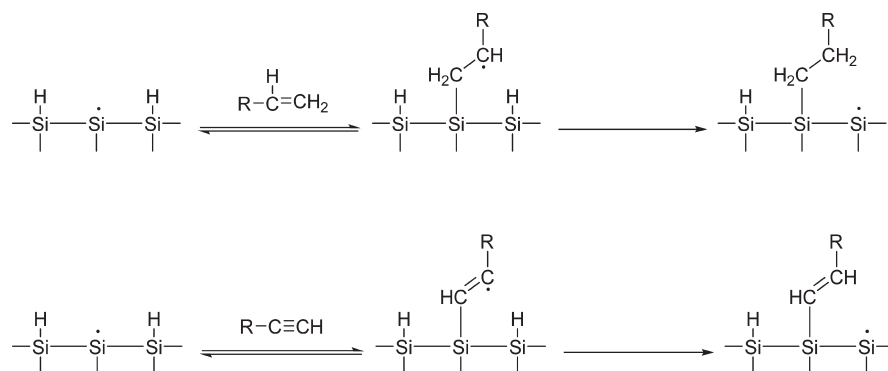
(a)

(b)

Figure 1. (a) Schematic of the potential energy landscape for the two-step hydrosilylation reaction. (b) Schematic showing typical kinetics observed for the hydrosilylation reaction on H-terminated c-Si surfaces.

H in a SiH$_4$ discharge. This H termination provides the necessary sites for further functionalization of Si NCs.

Previously, Si NCs with SiH$_x$-terminated ($x = 1-3$) surfaces have been functionalized with organic ligands primarily using ex situ liquid-phase techniques based on Grignard reagent chemistry and hydrosilylation.[17] A drawback of these techniques is that they involve numerous process steps, including transfer of Si NCs into the liquid phase, passivation of the NCs, and subsequent separation of the NCs out of the liquid phase.[3,20] Special precautions are required during each step to avoid adventitious moisture and oxygen in the process environment.[3,20] Furthermore, the separation of Si NCs < 5 nm out of the liquid phase and removal of the reaction byproducts can be challenging tasks, but ultimately reduce the process yield.

In situ gas-phase passivation of Si NCs can be a suitable alternative to liquid-phase passivation. In spite of the advantages of gas-phase functionalization, there are relatively few reports in the literature using this approach. Liao and Roberts demonstrated the gas-phase self-assembly of various organic monolayers on aerosolized ~12-nm-diameter Si NCs.[21] Mangolini and

Kortshagen used radicals generated in a hydrocarbon plasma for passivating the surface of Si NCs.[22] Nozaki et al. employed a single-step process to synthesize alkyl-terminated Si NCs using a SiCl$_4$/CH$_4$ plasma.[23] While gas-phase passivation has not been extensively investigated for Si NCs, gas-phase passivation via hydrosilylation has been well-studied on H-terminated c-Si wafer surfaces.[24−29] The surfaces of Si NCs are more complex, having several crystal orientations terminated with mono-, di-, and trihydrides and displaying different reactivity with 1-alkenes and 1-alkynes.[18,30,31] Despite these complications, we demonstrate here that gas-phase functionalzation can be successfully extended to Si NCs.

During gas-phase hydrosilylation, vapors of 1-alkenes or 1-alkynes are employed to passivate the surface of H-terminated c-Si with organic ligands. Hydrosilylation proceeds via a radical-chain mechanism, shown in Scheme 1.[31−29] In this two-step process, first, a 1-alkene or 1-alkyne chemisorbs onto a dangling bond on the surface and forms a metastable state, with the dangling bond transferred to the secondary C atom of the hydrocarbon chain. In the second step, an H atom is abstracted from a neighboring SiH site, resulting in a dangling bond on the Si surface, which provides a site for further chemisorption of the organic species (see Scheme 1). The corresponding potential energy landscape for this two-step reaction is shown in Figure 1a.[31] Generally, chemisorption of 1-alkene/1-alkyne on a dangling bond on the Si surface occurs with a negligible activation energy barrier.[31] After the first step, the metastable state is in a local energy minimum and can follow either of the following two pathways: H abstraction, resulting in successful hydrosilylation, or desorption of the chemisorbed hydrocarbon back into the gas phase. The two possible pathways compete with each other during hydrosilylation, and the rate of alkyl or alkenyl termination depends on the relative barrier heights for H abstraction and hydrocarbon desorption (see Figure 1a). Thus, in a two-step process that involves an intermediate metastable state, the c-Si surface can be terminated with organic ligands using the hydrosilylation reaction.

The kinetics of gas-phase hydrosilylation of Si surfaces proceeds via two distinct regimes where the rate of hydrosilylation decreases with time (see Figure 1b).[28,29] In Figure 1b, k_f and k_s are the effective rate coefficients for the fast and slow kinetic regimes, respectively. The first reason for the slower kinetics with time is explained by the self-avoiding random walk model on triangular lattices.[32] Initially, there are a finite number of dangling bonds on the surface, and each dangling bond site can initiate the
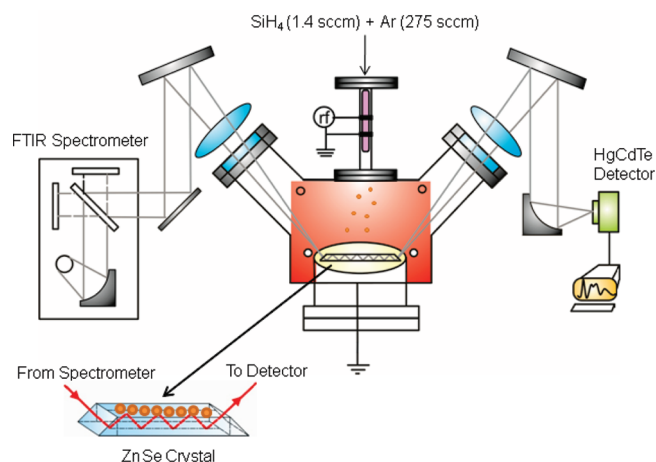
Figure 2. Schematic of the reactor setup showing the capacitively coupled nonthermal plasma attached to a high-vacuum surface analysis chamber equipped with in situ ATR-FTIR spectroscopy.

radical-chain mechanism. The model shows that as the chain reaction proceeds, after a certain number of steps, the hydrocarbon species chemisorbs onto a site that does not have any remaining H atoms bonded to a neighboring Si atom, which results in the self-termination of this chain process. Thus, slower kinetics is expected with increasing hydrocarbon coverage of the surface. A second reason for the decrease in the reaction rate is due to the corresponding increase in steric hindrance on the surface with increasing surface coverage of organic ligands. Therefore, as shown in Figure 1b, slower kinetics with time results in saturation surface coverage: the onset of this regime depends on the type of 1-alkene/1-alkyne, which determines the difference in the barriers for H abstraction versus hydrocarbon desorption back into the gas phase.

As mentioned earlier, gas-phase hydrosilylation has been extensively studied on H-terminated c-Si surfaces.[24−29] It has been shown that, in the case of short-chain linear alkenes such as ethylene and propylene, hydrosilylation on bulk c-Si surfaces does not occur,[26,31] and this has been attributed to a relatively high H-abstraction barrier compared to desorption of such alkenes.[31] On the other hand, successful hydrosilylation has been shown using long-chain alkenes including linear chain alkenes as well as aromatic compounds such as styrene.[25,26,31] Further, compared to alkenes, alkynes are known to be more reactive during hydrosilylation on c-Si surfaces.[30,31,33] The higher reactivity has been attributed to a relatively low H-abstraction barrier compared to alkenes with the same chain length, which is accompanied by a higher overall exothermicity of the reaction. This, in turn, is due to a higher nucleophilicity of alkynes, resulting in facile attack at the Si−H bond and due to the formation of an energetically more favorable metastable state owing to electron delocalization over the double bonds.[31,33] It has also been demonstrated that, unlike 1-alkenes, 1-alkynes react differently with SiH- and SiH_2-terminated Si(100) surfaces, forming alkyl monolayers instead of alkenyl monolayers:[18] this difference in reactivity can be utilized to enhance the overall surface coverage.

In this article, we present a novel pathway for in situ gas-phase hydrosilylation of plasma-synthesized Si NCs. We have employed real-time in situ attenuated total reflection Fourier transform infrared (ATR-FTIR) spectroscopy,[34,35] to observe the kinetics of the hydrosilylation reaction on Si NC surfaces. Using this kinetic data, we demonstrate a surface passivation route that results in significantly enhanced surface ligand coverage through the combination of a short-chain alkyne (acetylene) and a long-chain 1-alkene (styrene), which react preferentially with various surface hydrides. We further show that the enhanced surface coverage reduces the oxidation rate.

2. EXPERIMENTAL SECTION

2.1. Si NC Synthesis. Si NCs were synthesized using a capacitively coupled nonthermal plasma attached to a high-vacuum surface analysis chamber with a base pressure of $\sim 10^{-7}$ Torr (see Figure 2). The plasma was generated in a quartz tube (9.5 mm outer diameter and 7 mm inner diameter) surrounded by two Cu ring electrodes and powered by a rf generator (13.56 MHz) via an in-house-built matching network.[2] The spacing between the electrodes was 3 cm, with the powered electrode closer to the upstream end of the tube at a distance of 5 cm from the stainless steel quick-coupling flange. The feed gas was SiH_4 (1.4 sccm) heavily diluted in Ar (275 sccm) with a pressure of ~ 4 Torr measured close to the inlet of the quartz tube. The rf power to the plasma source was set at 35 W to obtain crystalline nanoparticles.[36] The NCs nucleated in the gas phase and were transported out of the plasma by convective flow. For each experiment, the plasma-on time was 6 s. After each NC growth and passivation step, the quartz tube was removed and cleaned with a 1 M KOH solution to etch the Si film and the Si NCs deposited on the inner walls of the tube.

2.2. In Situ Surface IR Spectroscopy. The Si NC synthesis reactor was attached to a high-vacuum chamber equipped with an in situ ATR-FTIR spectroscopy setup shown in Figure 2.[34,35] A trapezoidal ZnSe internal reflection crystal (IRC) with dimensions 1 mm × 10 mm × 50 mm and the short faces beveled at 45° was placed in the line of sight with the axis of the cylindrical quartz tube such that the NCs were directly collected on the IRC. An IR beam from a FTIR spectrometer (Nicolet 6700) was focused onto the beveled edge of the IRC at an angle greater than the critical angle for total internal reflection. The IR beam undergoes 25 reflections on the top and bottom faces of the IRC. The exiting beam from the opposite beveled edge was collimated using a KBr lens and directed by a series of mirrors onto a mercury−cadmium−telluride (MCT-A) detector. We chose ZnSe as the IRC because it is transparent in the IR up to ~ 700 cm^{-1}, which allowed us to simultaneously observe the $\sim CH_x$ ($x = 1-3$) stretching modes in the ~ 3000 cm^{-1} region, the SiH_x ($x = 1-3$) stretching modes in the 2100 cm^{-1} region, and the SiH_x ($x = 2$ and 3) scissor modes in the ~ 900 cm^{-1} region. A c-Si wafer was placed adjacent to the ZnSe IRC to simultaneously collect a fraction of the Si NCs. Both substrates were preheated to 160 °C prior to turning on the SiH_4/Ar plasma. After each Si NC synthesis and hydrosilylation experiment, a clean quartz tube was installed, and a SF_6 plasma was used to etch the passivated Si NCs deposited on the IRC. The SF_6 discharge was created in a parallel-plate geometry within the high-vacuum chamber. Radio-frequency power at 13.56 MHz was applied to a rectangular stainless steel plate, while the heated substrate served as the grounded electrode.[34] The plasma cleaning step was monitored by collecting IR spectra and observing the disappearance of the CH_x ($x = 1-3$) and SiH_x ($x = 1-3$) stretching vibrations to ensure that all of the Si NCs on the IRC were etched away.

2.3. Gas-Phase Hydrosilylation and Oxidation of Si NCs. Thermal hydrosilylation was performed on the Si NCs at 160 °C with the precursors supplied through the gas phase. The hydrosilylation reaction was studied for three different cases: (a) styrene, (b) acetylene, and (c) a sequential exposure to acetylene and styrene. To observe the changes in the bonding configurations on the surface during hydrosilylation, two reference spectra were collected: one for the bare IRC and the second with the NCs deposited onto the IRC. Thus, depending on
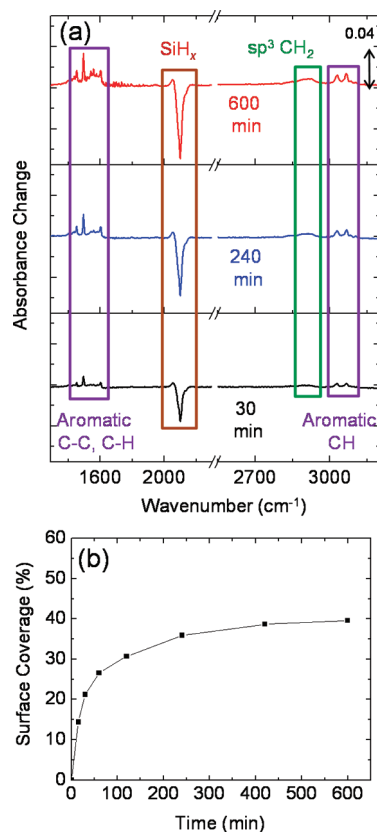
Figure 3. (a) IR difference spectra of Si NCs during styrene exposure at 160 °C. (b) Temporal evolution of the surface coverage during styrene exposure of Si NCs.

Scheme 2. H Abstraction during Styrene Hydrosilylation Resulting in Functionalization of the Si Surface with a Styrene Molecule

the background spectrum, each IR spectrum collected thereafter directly represents the changes that occur on the surface with respect to either the bare IRC or the as-deposited Si NCs. Acetylene (96% purity) was introduced into the chamber using a mass flow controller set at 250 sccm, and the chamber was maintained at a pressure of ~275 ± 10 mTorr using a manual gate valve. For styrene (99.8% purity) exposure, the precursor was introduced into the vacuum chamber from a metal container through a needle valve, while maintaining a pressure of ~275 ± 10 mTorr. In the case where a combination of acetylene and styrene was employed, the Si NCs were initially exposed to acetylene for 180 min, followed by styrene for 495 min, at the pressures mentioned above. Because ATR-FTIR spectroscopy is sensitive to gas-phase species as well, the IR spectra were collected after turning off the acetylene/styrene flow and pumping out the gas-phase hydrocarbons completely. The oxidation of passivated and H-terminated Si NCs was also studied using in situ ATR-FTIR spectroscopy. After hydrosilylation, the chamber was opened to the atmosphere and IR spectra were collected after 1 and 3 days while monitoring the change in the SiH_x ($x = 1-3$) stretching region due to oxidation. For IR spectra acquisition during oxidation, the chamber was again pumped out to eliminate H_2O and CO_2 in the IR beam path. To study the oxidation using PL spectroscopy, the Si NCs were deposited for 5 min on a Si wafer placed next to the ZnSe IRC. A 5-min deposition was necessary in order to obtain measurable PL from the Si NCs at room temperature. A 514.5-nm excitation from an Ar^+ laser was used as the excitation source, and the spectra were recorded ex situ over a wavelength range of 516−1081 nm using a Si CCD detector.

3. RESULTS AND DISCUSSION

3.1. Styrene Hydrosilylation of Si NCs.
Surface hydrosilylation through the gas phase with styrene has been well studied on
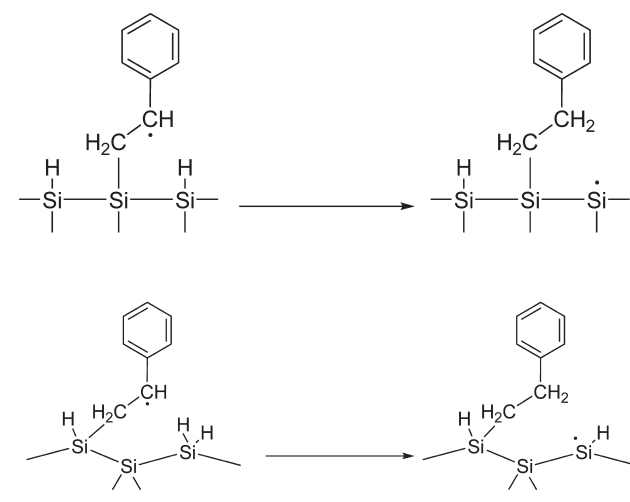
Si(111) and Si(100) surfaces, which provides a suitable benchmark for our experiments.[25,26,31,37,38] Previously, we characterized the as-synthesized Si NCs (<5 nm) obtained using the same plasma-assisted process showing that the surface was highly faceted and terminated with mono-, di-, and trihydrides.[36] IR difference spectra recorded during styrene hydrosilylation performed on Si NCs are shown in Figure 3, with the corresponding reaction mechanisms illustrated in Scheme 2. Thus, in Figure 3, any increase in absorbance indicates the creation of new species on the surface, and a decrease in absorbance indicates the removal of surface species, or their reaction with styrene. Chemisorption of styrene on the Si NC surface can be inferred from the increase in absorbance for the peaks at ~3029 and ~3064 cm^{-1} corresponding to the C−H stretching vibrations in the aromatic ring and the ~1490−1600 cm^{-1} region corresponding to the various aromatic C−C stretching modes and the in-plane bending mode of the aromatic C−H bonds present in styrene.[39] The band from ~2850−2940 cm^{-1} corresponds to the antisymmetric and symmetric sp^3 CH$_2$ stretching modes,[40] indicating conversion of olefinic sp^2 CH in styrene to sp^3 CH$_2$ via neighboring H-atom abstraction during hydrosilylation of the NC surface. The absence of peaks at ~2982 and ~1630 cm^{-1} corresponding to sp^2 CH and C=C stretching modes, respectively,[39] shows that there is no unreacted styrene on the surface. In Figure 3a, a corresponding decrease in the SiH_x ($x = 1-3$) stretching region at 2100 cm^{-1} indicates that H is abstracted from all surface hydrides present on the NCs. However, there is a slight increase in absorbance at ~2070 cm^{-1} corresponding to the SiH stretching vibrations, which will be discussed in section 3.3. The decrease in SiH_x ($x = 1-3$) stretching vibrations is not due to thermal desorption of the surface H atoms at 160 °C: NCs heated in the absence of styrene show <5% change in absorbance over a period of 6 h and practically no change in absorbance after 2 h.

It is difficult to quantify the surface styrene coverage using IR spectra because (a) the IR absorption cross section for various C−C and C−H vibrations depends on the local bonding environment and (b) the total surface area of the NCs is unknown. During hydrosilylation, every styrene molecule chemisorption event corresponds to an H-atom abstraction event from a neighboring SiH_x ($x = 1-3$) site (see Scheme 2). Therefore, to directly determine the surface coverage of organic
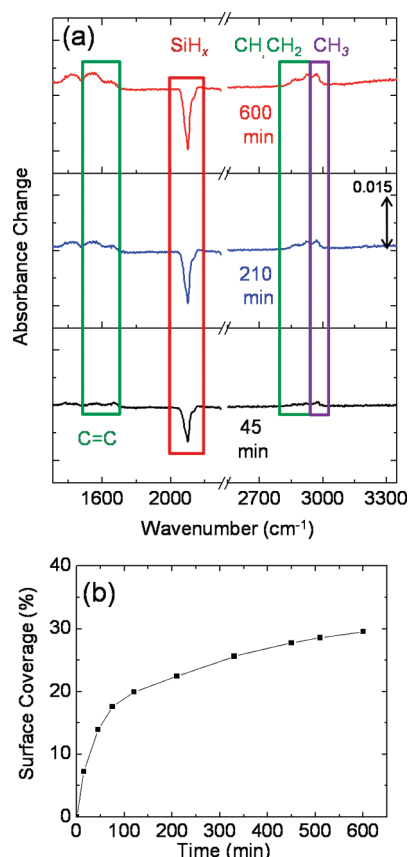
Figure 4. (a) IR difference spectra of Si NCs during acetylene exposure at 160 °C. (b) Temporal evolution of the surface coverage during acetylene exposure of Si NCs.

ligands, θ_s, we have used the fractional decrease in the integrated absorbance of the SiH_x ($x = 1-3$) stretching band in the ~ 2100 cm^{-1} region, which is given by

$$\theta_s = \frac{IA_{SiH_{x,t=0}} - IA_{SiH_{x,t}}}{IA_{SiH_{x,t=0}}} \quad (1)$$

In eq 1, $IA_{SiH_{x,t}}$ is the integrated absorbance at any given time t, obtained directly from the difference spectra in Figure 3a, and $IA_{SiH_{x,t=0}}$ is obtained from the IR spectrum for the as-synthesized Si NCs. Because the initial surface H coverage has been reported close to 95% for similarly synthesized Si NCs, this method gives a reasonably accurate measure of the surface ligand coverage.[41] Figure 3b plots the temporal evolution of the surface coverage during the hydrosilylation reaction. The kinetics of hydrosilylation on Si NCs is similar to that observed on c-Si wafer surfaces, where initially the surface coverage increases rapidly during the fast kinetic regime and slows down as it enters the slow kinetic regime (see Figure 1). A maximum surface coverage of $\sim 38\%$ was obtained using styrene termination on Si NCs.

3.2. Acetylene Hydrosilylation of Si NCs. Hydrosilylation of Si NCs using short-chain hydrocarbons has not been explored previously. We chose the shortest chain unsaturated hydrocarbons, ethylene and acetylene, to study the hydrosilylation of Si NCs because short-chain hydrocarbons are expected to reduce the steric hindrance on the surface. With ethylene, hydrosilylation of Si NC surfaces was not successful because of a really low reaction rate observed in our IR data. As explained earlier (see

Scheme 3. H-Abstraction Mechanism during Acetylene Hydrosilylation Resulting in (a) Alkenyl Termination on a SiH-Terminated Surface, (b) a 1−1 Bridge Structure, (c) a 1−2 Bridge Structure on a SiH₂-Terminated Surface, and (d) a Polyacetylene-Like Structure on a SiH₂-Terminated Surface
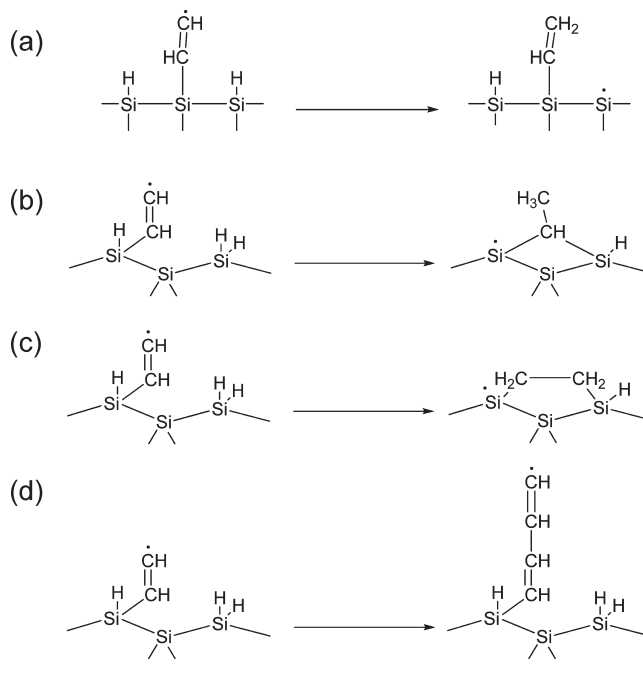

Figure 1), a possible reason for the low reaction rate could be a higher barrier for abstraction in comparison with desorption of ethylene back into the gas phase, as demonstrated previously for ethylene chemisorption the an H-terminated Si(111) surface.[31] The calculations in ref 31, however, predict a deeper local minimum for acetylene and an energetically favorable pathway toward hydrosilylation, which was also observed in our experiments. Figure 4 shows the temporal evolution of the IR difference spectra and the surface coverage during acetylene exposure of Si NCs. As in the case of styrene hydrosilylation, H-atom abstraction from different surface hydrides is indicated by the decrease in absorbance in the SiH_x ($x = 1-3$) stretching region, which is used to calculate the fractional surface ligand coverage. A corresponding increase in absorbance at ~ 1600 and ~ 2900 cm^{-1} indicates termination of the NC surface with acetylene. Specifically, the broad band at ~ 2900 cm^{-1} can be assigned to the sp^3-hybridized CH ($\sim 2880-2900$ cm^{-1}), sp^2-hybridized CH (~ 2980 cm^{-1}), sp^2-hybridized CH$_2$ (~ 3010 cm^{-1}), and antisymmetric/symmetric sp^3-hybridized CH$_2$ and CH$_3$ ($\sim 2845-2965$/$\sim 2915-2935$ and $\sim 2860-2880$/ $2950-2970$ cm^{-1}, respectively).[39,40] The broad band at ~ 1600 cm^{-1} consists of the olefinic sp^2 C=C stretching mode centered at ~ 1630 cm^{-1},[40] indicating alkenyl termination via the mechanism shown in Scheme 3a. Unlike alkenes, alkynes react through different pathways with mono- and dihydride-terminated Si surfaces. Parts b−d of Scheme 3 show three other distinct mechanisms for the hydrosilylation of mono- and dihydride-terminated Si surfaces with acetylene. The presence of the absorption bands at ~ 2930 and ~ 2970 cm^{-1}, corresponding to the antisymmetric stretching modes of sp^3-hybridized CH$_2$ and CH$_3$,[40] clearly shows that acetylene undergoes bis-silylation and forms 1−1 and 1−2 bridged structures[18] while reacting with SiH$_2$ on the NC
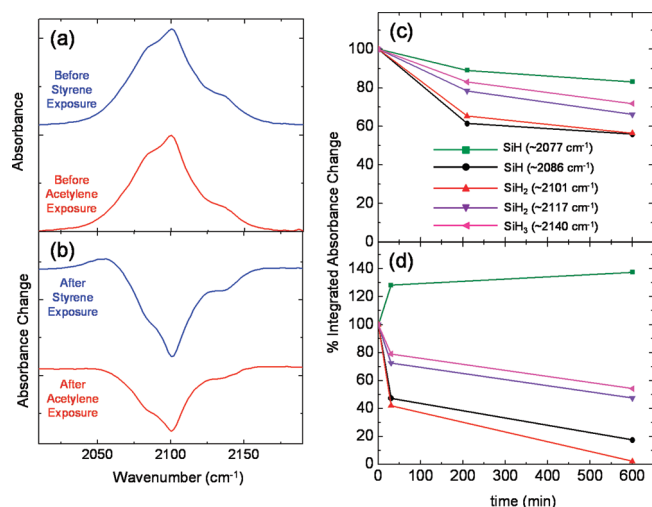
Figure 5. (a) Absorbance in the SiH$_x$ ($x = 1-3$) stretching region for as-synthesized Si NCs before styrene (blue) and acetylene (red) exposure. The reference spectrum is for a bare IRC. (b) Difference spectra showing the SiH$_x$ ($x = 1-3$) stretching region for NCs after 600 min of styrene (blue) and acetylene (red) exposure. The reference spectrum was recorded after NC deposition onto the IRC. Temporal evolution of the integrated absorbance change for the SiH$_x$ ($x = 1-3$) species with respect to the as-deposited Si NCs for (c) acetylene-exposed NCs and (d) styrene-exposed NCs.

surface, as shown in parts b and c of Scheme 3. The absorption band at ∼1600 cm^{-1} also contains a peak centered at ∼1560 cm^{-1} corresponding to conjugated olefinic C≡C bonds. Previous calculations by Martinez-Guerra and Takeuchi have shown that polymerization of acetylene molecules on the dihydride-terminated Si surface has a similar activation energy compared to H abstraction from a neighboring Si—H bond.[42] Therefore, the peak at ∼1560 cm^{-1} is attributed to the formation of a polyacetylene-like structure via the mechanism shown in Scheme 3d. Thus, we conclude that acetylene and styrene react differently with the Si NC surface, and this difference in reactivity can be used to enhance the overall surface ligand coverage through a combination of alkenes and alkynes as the passivating agents. It is, however, not possible to quantify the fraction of acetylene molecules reacting with the surface via different pathways because the IR absorption cross sections for various C—H stretching vibrations in different surface environments are not known.

The surface coverage of acetylene, calculated using eq 1 and its kinetics, is shown in Figure 4b. Although the kinetic behavior is similar to that of hydrosilylation via styrene, a maximum surface coverage of ∼30% was obtained. Alkynes are considered more reactive than alkenes only when compared to alkenes with the same chain length. Therefore, a reason for a lower surface coverage than with styrene could be the shorter chain length of acetylene compared to styrene. Further, as mentioned above, acetylene can also undergo a polymerization-type reaction on the surface, resulting in conjugated olefinic C≡C bonds. This process of polymerization also competes with the acetylene termination, resulting in slower kinetics and lower surface coverage relative to styrene. Finally, the bridged compounds that result could produce similar, or even more, steric congestion than the aryl group of adsorbed styrene. In the proposed reaction schemes, formation of the bridged compounds generates a dangling bond on a Si atom to which the organic is bound.

Scheme 4. H-Abstraction Mechanism during Styrene Hydrosilylation Resulting in the Formation of SiH on a SiH$_2$-Terminated Surface[a]
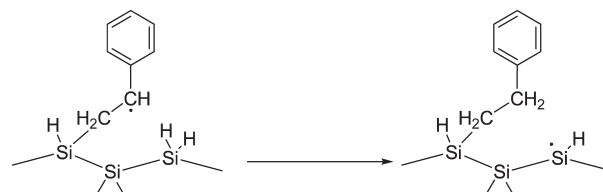
[a] Further H abstraction from such SiH sites is relatively difficult because of steric hindrance effects.
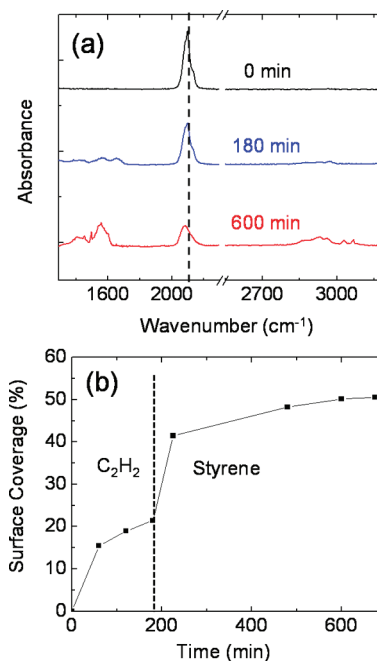

Figure 6. (a) IR absorbance spectrum of as-synthesized NCs (black), followed by 180 min of C$_2$H$_2$ exposure (blue) and 420 min of styrene exposure (red) at 160 °C. The reference spectrum is for a bare IRC. The dotted line is to emphasize the shift in the peak of the SiH$_x$ ($x = 1-3$) stretching region toward lower wavenumbers after styrene exposure. (b) Temporal evolution of the surface coverage during sequential acetylene and styrene exposure of Si NCs.

The adsorbed organic might block this site from further reaction. Similar sites are not produced by reaction with styrene.

3.3. Combination of Acetylene and Styrene Hydrosilylation of Si NCs. After studying hydrosilylation via styrene and acetylene, we employed a combination of the two passivating agents to increase the surface coverage as hypothesized above. Figure 5a shows the IR absorbance spectra of the Si NCs before hydrosilylation with styrene (blue) and acetylene (red). These IR spectra show that the initial SiH$_x$ ($x = 1-3$) compositions of the Si NCs in both experiments are almost identical. The corresponding difference spectra after 600 min of styrene (blue) and acetylene (red) exposure are shown in Figure 5b. To quantify the noticeable difference in the absorbance spectra in the two experiments, absorbance spectra at different time intervals during hydrocarbon exposure were deconvoluted using peak assignments from our previous work,[36] and a temporal evolution of individual surface hydride absorption bands was studied. Parts c and d of Figure 5

Table 1. Surface Coverages and Percent Changes in the SiH$_x$ (x = 1−3) Stretching Regions after 1 and 3 Days for Different Passivating Agents

passivating agent	hydrosilylation surface coverage (%)	first day oxidation (% SiH$_x$ change)	third day oxidation (% SiH$_x$ change)
acetylene	∼30	∼37	
styrene	∼38	∼12	∼18
acetylene + styrene	∼50	∼9	∼13

Figure 7. Normalized PL spectra of (a) as-synthesized NCs and (b) styrene-passivated NCs exposed to the atmosphere.

show the relative change in the integrated absorbance of surface SiH$_x$ (x = 1−3) absorption modes during acetylene and styrene exposure, respectively. In the case of acetylene, there is a decrease in all of the different surface hydrides present on the NCs. However, during styrene exposure, there is an increase in absorbance for the SiH mode centered at ∼2077 cm^{-1}. This band corresponds to SiH, similar to that observed at steps on chemically prepared rough Si(100) and Si(111) surfaces.[43] Moreover, the change in the absorbance due to SiH$_2$ and SiH$_3$ is relatively fast during styrene exposure compared to acetylene. The reason for the increase in the SiH mode at ∼2077 cm^{-1} is a relatively fast abstraction rate from SiH$_2$ and SiH$_3$ by styrene, resulting in the formation of surface SiH sites, as shown in Scheme 4. Further H abstraction from these SiH sites by incoming styrene might be relatively unlikely because of steric hindrance effects.

The results of combined acetylene and styrene hydrosilylation are shown in Figure 6. Figure 6a shows the IR absorbance spectra of as-synthesized Si NCs (black) and Si NCs after 180 min of acetylene exposure (blue), followed by 420 min of styrene exposure (red). The reference spectrum in each spectrum is for a bare IRC. A clear shift in the SiH$_x$ (x = 1−3) absorption band peak intensity toward lower wavenumbers is apparent in the spectra, indicating that after acetylene and styrene exposure the NC surface is dominated with monohydrides. Although H abstraction occurs from all surface hydrides, this shift can be attributed to the conversion of SiH$_2$ and SiH$_3$ sites to SiH via H abstraction during acetylene and styrene chemisorption.

The temporal evolution of the surface ligand coverage is shown in Figure 6b. After a total exposure time of 600 min, which is the same as individual acetylene and styrene hydrosilylation experiments, the total surface coverage was ∼50%. This surface coverage is significantly greater than that obtained using acetylene or styrene individually. Additional exposure to styrene beyond 600 min shows the surface coverage reaching saturation. The kinetic data in Figure 6b show that initially when acetylene was introduced, as expected, it reacted rapidly with the surface hydrides in the fast kinetic regime. When the acetylene hydrosilylation reaction entered the slow kinetic regime (∼180 min), acetylene exposure was stopped and styrene was introduced into the chamber. The introduction of styrene results in a rapid initial increase in the surface coverage because at ∼20% ligand coverage styrene still follows the fast kinetic regime (see Figure 3b). In the sequential exposure, the fast kinetic regime for styrene is expected to continue to a higher surface coverage because the steric hindrance on the surface is lower due to the short-chain alkenyl termination of ∼20% of the surface sites. This is indeed what we observed; the fast kinetic regime continues until ∼40% surface coverage (Figure 6b) as compared to ∼30% for just styrene exposure (Figure 3b). If styrene is introduced prior to acetylene, it would consume a larger fraction of the surface
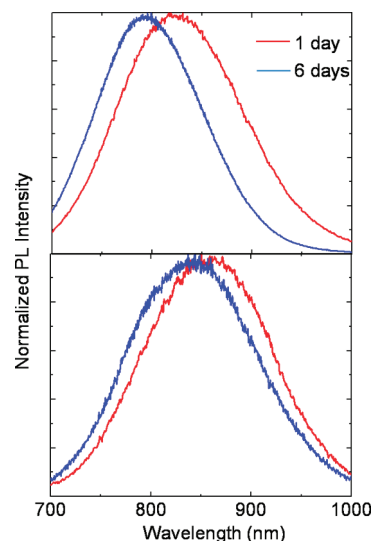
hydrides in the fast regime, resulting in the initiation of acetylene hydrosilylation in the slower kinetics regime (see the Supporting Information, Figure S1). Therefore, only using the combination of a short-chain alkyne followed by a longer chain alkene, enhanced surface passivation was observed.

3.4. Oxidation of Passivated Si NCs. Surface oxidation of the passivated Si NCs during exposure to air was also studied using in situ ATR-FTIR spectroscopy. Three primary reactions previously observed during oxidation of H-terminated Si surfaces are (a) O atom insertion in Si−Si back-bonds resulting in O$_y$SiH$_x$ (x, y = 1−3) sites, (b) formation of a Si−O−Si bond, and (c) O atom insertion in Si−H bonds resulting in SiOH sites.[44,45] The formation of O$_y$SiH$_x$ (x, y = 1−3) sites results in a shift in the stretching modes of SiH$_x$ species to higher frequencies, ∼150−200 cm^{-1}.[45] The formation of SiOH results in a decrease in the integrated absorbance of the SiH$_x$ (x = 1−3) modes.[45] There is a also an increase in absorbance centered at ∼1050 cm^{-1} attributed to Si−O−Si transverse optical antisymmetric stretching vibrations due to the formation of SiO$_2$.[36] Therefore, the stability of the hydrocarbon-terminated Si NCs against oxidation can be related to the stability of the remaining surface SiH$_x$ (x = 1−3) bonds in air. Table 1 shows the percent change in absorbance in the SiH$_x$ (x = 1−3) stretching region due to atmospheric oxidation of Si NCs with different surface coverages obtained during the three types of hydrosilylation experiments discussed in previous sections. It is clear from the data in Table 1 that increasing in the surface coverage leads to enhanced surface passivation and resistance to oxidation.

Ex situ PL measurements performed to study the atmospheric oxidation of as-synthesized and styrene-terminated NCs corroborate the in situ IR measurements. To obtain sufficient PL intensity at room temperature, the Si NCs were deposited for 5 min. A longer exposure time of ∼780 min was employed to terminate the NCs with styrene. In situ IR measurements showed that the saturation surface coverage (∼38%) did not change compared to styrene hydrosilylation on Si NCs deposited for only 6 s. Figure 7 shows the normalized PL spectra of as-synthesized and styrene-terminated Si NCs exposed to air for periods of 1 and 6 days. The blue shift in the PL spectra

corresponds to the decrease in the NC size resulting from oxidation.[46] For styrene-terminated NCs, the PL shift after 6 days was ~12 nm compared to ~30 nm for as-synthesized NCs. The PL measurements indicate that styrene termination indeed decreases the rate of oxidation of Si NCs.

4. CONCLUSIONS

In conclusion, we have demonstrated the surface functionalization of plasma-synthesized H-terminated Si NCs via a two-step in situ gas-phase hydrosilylation chemistry, which accomplishes a high-degree of surface functionalization and reduces the number of process steps compared to liquid-phase routes. For a single-step process, maximum surface coverages of ~38% and ~30% were observed in the case of styrene and acetylene hydrosilylation, respectively. The mechanism for hydrosilylation using acetylene was significantly different compared to styrene. During styrene hydrosilylation, H atoms were preferentially abstracted from di- and trihydride sites. However, in the case of acetylene, H atoms were abstracted from all surface hydride species. For acetylene, along with the expected alkenyl termination, IR peaks indicating 1−1 and 1−2 bridge structures via bis-silylation were also observed. On the basis of this difference in the reactivity of 1-alkenes and 1-alkynes, we demonstrated a novel in situ gas-phase hydrosilylation process for Si NCs using a combination of acetylene and styrene, which results in a maximum surface coverage of ~50%. To obtain such high coverage, it was important to select the proper sequence in which the NCs were exposed to acetylene and styrene. Because acetylene is a relatively small molecule, styrene reacts faster than acetylene with the surface hydrides. Therefore, the introduction of acetylene before styrene during the fast kinetic regime was necessary to obtain a higher surface coverage. The PL spectra indicate that an increase in the surface coverage of the organic ligands increases the resistance of Si NCs to oxidation in air. Although other combinations of 1-alkynes and 1-alkenes may result in an even higher surface coverage, perhaps close to the theoretically predicted maximum of ~69% on flat c-Si,[47] our experiments, nonetheless, illustrate the key finding that hydrosilylation performed by employing a short-chain alkyne followed by a long-chain alkene results in a greater degree of passivation of Si NCs.

ASSOCIATED CONTENT

Ⓢ Supporting Information. Temporal evolution of the surface coverage during sequential styrene and acetylene exposure of Si NCs. This material is available free of charge via the Internet at http://pubs.acs.org.

AUTHOR INFORMATION

Corresponding Author
*E-mail: sagarwal@mines.edu (S.A.), cciobanu@mines.edu (C.V.C.).

ACKNOWLEDGMENT

REFERENCES

(1) Reboredo, F. A.; Franceschetti, A.; Zunger, A. *Phys. Rev. B* **2000**, *61*, 13073.

(2) Mangolini, L.; Thimsen, E.; Kortshagen, U. *Nano Lett.* **2005**, *5*, 655.

(3) Jurbergs, D.; Rogojina, E.; Mangolini, L.; Kortshagen, U. *Appl. Phys. Lett.* **2006**, *88*.

(4) de Boer, W.; Timmerman, D.; Dohnalova, K.; Yassievich, I. N.; Zhang, H.; Buma, W. J.; Gregorkiewicz, T. *Nat. Nanotechnol.* **2010**, *5*, 878.

(5) Beard, M. C.; Knutsen, K. P.; Yu, P. R.; Luther, J. M.; Song, Q.; Metzger, W. K.; Ellingson, R. J.; Nozik, A. J. *Nano Lett.* **2007**, *7*, 2506.

(6) Murphy, C. J.; Coffer, J. L. *Appl. Spectrosc.* **2002**, *56*, 16A.

(7) Hirschman, K. D.; Tsybeskov, L.; Duttagupta, S. P.; Fauchet, P. M. *Nature* **1996**, *384*, 338.

(8) Pavesi, L.; Dal Negro, L.; Mazzoleni, C.; Franzo, G.; Priolo, F. *Nature* **2000**, *408*, 440.

(9) Li, Z. F.; Ruckenstein, E. *Nano Lett.* **2004**, *4*, 1463.

(10) Sailor, M. J.; Lee, E. J. *Adv. Mater.* **1997**, *9*, 783.

(11) Holec, T.; Chvojka, T.; Jelinek, I.; Jindrich, J.; Nemec, I.; Pelant, I.; Valenta, J.; Dian, J. *Mater. Sci. Eng., C* **2002**, *19*, 251.

(12) Timmerman, D.; Gregorkiewicz, T. *Mater. Sci. Eng., B* **2009**, *159−60*, 87.

(13) Svrcek, V.; Slaoui, A.; Muller, J. C. *Thin Solid Films* **2004**, *451*, 384.

(14) Liu, C. Y.; Holman, Z. C.; Kortshagen, U. R. *Nano Lett.* **2009**, *9*, 449.

(15) Puzder, A.; Williamson, A. J.; Grossman, J. C.; Galli, G. *J. Am. Chem. Soc.* **2003**, *125*, 2786.

(16) Anthony, R.; Kortshagen, U. *Phys. Rev. B* **2009**, *80*.

(17) Veinot, J. G. C. *Chem. Commun.* **2006**, 4160.

(18) Buriak, J. M. *Chem. Rev.* **2002**, *102*, 1271.

(19) Seto, T.; Kawakami, Y.; Suzuki, N.; Hirasawa, M.; Aya, N. *Nano Lett.* **2001**, *1*, 315.

(20) Mangolini, L.; Jurbergs, D.; Rogojina, E.; Kortshagen, U. *J. Lumin.* **2006**, *121*, 327.

(21) Liao, Y. C.; Roberts, J. T. *J. Am. Chem. Soc.* **2006**, *128*, 9061.

(22) Mangolini, L.; Kortshagen, U. *Adv. Mater.* **2007**, *19*, 2513.

(23) Nozaki, T.; Nakamuta, T.; Sagawa, M.; Okazaki, K. *J. Plasma Fusion Res.* **2009**, *8*, 500.

(24) Hossain, M. Z.; Kato, H. S.; Kawai, M. *J. Am. Chem. Soc.* **2007**, *129*, 3328.

(25) Cicero, R. L.; Chidsey, C. E. D.; Lopinski, G. P.; Wayner, D. D. M.; Wolkow, R. A. *Langmuir* **2002**, *18*, 305.

(26) Lopinski, G. P.; Wayner, D. D. M.; Wolkow, R. A. *Nature* **2000**, *406*, 48.

(27) Tong, X.; DiLabio, G. A.; Wolkow, R. A. *Nano Lett.* **2004**, *4*, 979.

(28) Kosuri, M. R.; Gerung, H.; Li, Q. M.; Han, S. M.; Bunker, B. C.; Mayer, T. M. *Langmuir* **2003**, *19*, 9315.

(29) Kosuri, M. R.; Gerung, H.; Li, Q. M.; Han, S. M.; Herrera-Morales, P. E.; Weaver, J. F. *Surf. Sci.* **2005**, *596*, 21.

(30) Ng, A.; Ciampi, S.; James, M.; Harper, J. B.; Gooding, J. J. *Langmuir* **2009**, *25*, 13934.

(31) Takeuchi, N.; Kanai, Y.; Selloni, A. *J. Am. Chem. Soc.* **2004**, *126*, 15890.

(32) Cicero, R. L.; Linford, M. R.; Chidsey, C. E. D. *Langmuir* **2000**, *16*, 5688.

(33) Scheres, L.; Giesbers, M.; Zuilhof, E. *Langmuir* **2011**, *26*, 10924.

(34) Jariwala, B. N.; Ciobanu, C. V.; Agarwal, S. *J. Appl. Phys.* **2009**, *106*, 073305.

(35) Rai, V. R.; Agarwal, S. *J. Phys. Chem. C* **2009**, *113*, 12962.

(36) Jariwala, B. N.; Kramer, N. J.; Petcu, M. C.; van de Sanden, M. C. M.; Stradins, P.; Ciobanu, C. V.; Agarwal, S. *J. Phys. Chem. C* **2011** submitted for publication.

(37) Pei, Y.; Ma, J. *Langmuir* **2006**, *22*, 3040.

(38) Takeuchi, N.; Kanai, Y.; Selloni, A. *J. Phys. Chem. C* **2010**, *114*, 3981.

(39) Choi, C. H.; Kertesz, M. *J. Phys. Chem. A* **1997**, *101*, 3823.

(40) Coates, J. In *Encyclopedia of Analytical Chemistry*; Meyers, R. A., Ed.; Wiley: New York, 2000; p 10815.

(41) Mangolini, L.; Kortshagen, U. *Phys. Rev. E* **2009**, *79*, 026405.

(42) Martinez-Guerra, E.; Takeuchi, N. *Phys. Rev. B* **2007**, 75.

(43) Chabal, Y. J. *Physica B* **1991**, *170*, 447.

(44) Miura, T.; Niwano, M.; Shoji, D.; Miyamoto, N. *J. Appl. Phys.* **1996**, *79*, 4373.

(45) Mawhinney, D. B.; Glass, J. A.; Yates, J. T. *J. Phys. Chem. B* **1997**, *101*, 1202.

(46) Pi, X. D.; Mangolini, L.; Campbell, S. A.; Kortshagen, U. *Phys. Rev. B* **2007**, 75.

(47) Sieval, A. B.; Hout, B. v. d.; Zuilhof, H.; Sudhölter, E. J. R. *Langmuir* **2001**, *17*, 2172.